# LDPC-coded OFDM in fiber-optics communication systems [Invited]

**Ivan B. Djordjevic* and Bane Vasic**

*Department of Electrical and Computer Engineering, University of Arizona, 1230 E. Speedway Boulevard, Tucson, Arizona 85721, USA*
**Corresponding author: ivan@ece.arizona.edu*

Received September 27, 2007; revised January 5, 2008; accepted January 7, 2008; published February 22, 2008 (Doc. ID 88006)

Low-density parity-check (LDPC) coded orthogonal-frequency-division multiplexing (OFDM) is studied as an efficient coded modulation technique suitable for fiber-optics communication systems. We show that in long-haul fiber optics communications LDPC-coded OFDM increases spectral efficiency and requires simple equalization to deal with chromatic dispersion. LDPC-coded OFDM is also a promising polarization-mode dispersion compensation technique. Several power efficient OFDM schemes and LDPC codes suitable for use in LDPC-coded OFDM optical communication systems are discussed.

*OCIS codes:* 060.2330, 060.4080, 060.4230.

## 1. Introduction

Orthogonal-frequency-division multiplexing (OFDM) [1–15] is a multicarrier transmission scheme in which a single information-bearing stream is transmitted over many lower rate subchannels. OFDM has already been used in a variety of applications including digital audio broadcasting [1], high-definition television (HDTV) broadcasting [2], high bit-rate digital subscriber line (DSL), asymmetric DSL and very high data rate DSL, IEEE 802.11, and multimedia mobile access communications wireless local area networks (LANs) [1]. It has recently been proposed for use in radio-over-fiber-based links [3], in free-space optical communications [4,5], in long-haul optical communications systems [6–8], in multimode fiber links [9], in plastic optical fiber (POF) links [10], and as a multiplexing method to enable 100 Gbits/s Ethernet [11]. Due to the orthogonality among subcarriers in OFDM, partial overlap of neighboring frequency slots is allowed, thereby improving spectral efficiency as compared with a conventional multicarrier system. Also, by using a sufficiently large number of subcarriers and cyclic extension, the intersymbol interference (ISI) due to chromatic dispersion can be significantly reduced [6,14,15]. We have recently shown [12] (see also [13]) that the low-density parity-check (LDPC)-coded OFDM provides very good polarization-mode dispersion (PMD) compensation, capable of differential-group delay (DGD) compensation on the order of 1500 ps and above! Notice that the LDPC-coded turbo PMD equalizer proposed in [16] is suitable for DGD compensation up to 300 ps (at 10 Giga symbols/s) if the complexity of the turbo equalizer is to be kept reasonably low.

In this invited paper we show that LDPC-coded OFDM is an efficient coded modulation technique suitable for use in long-haul fiber-optics communications (i) to increase the spectral efficiency, (ii) for chromatic dispersion compensation, and (iii) for PMD compensation. Dominant limiting factors affecting the performance of high bit-rate return-to-zero on–off keying (RZ-OOK) systems operating at 40 Giga symbols/s and above are intrachannel four-wave mixing (IFWM) and intrachannel cross-phase modulation (IXPM) [17]. Because in OFDM a high-data rate data stream is split into a number of low-rate data streams that are transmitted simultaneously over a number of subcarriers, the 40 Gbits/s aggregate date rate can be divided among many subcarriers, and since the per channel OFDM symbol rate is much lower, the intrachannel nonlinearities present in on–off keying (OOK) transmission can be completely avoided. On the other hand, in OFDM systems four-ware mixing (FWM) between different subcarriers is an important factor in performance degradation. A careful design of the OFDM systems is necessary to exploit the advantages of the OFDM such as

insensitivity to chromatic dispersion and PMD and minimize degradation due to FWM of subcarrier terms.

Another possible application of LDPC-coded OFDM includes 100 Gbits/s Ethernet. Ethernet was initially introduced as a communication standard for short-distance connection among hosts in LANs [18–20]. However, due to its low cost, high speed, and simplicity compared to other protocols, it has been rapidly evolved, and network interface cards (NICs) for 1 and 10 Gbits/s Ethernet are already commercially available [19]. Because Ethernet data rates have traditionally grown in 10× increments, data rates of 100 Gbits/s are being envisioned for the next generation [18–20]. Despite the recent progress in high-speed electronics, electrical time division multiplexing modulators and photodetectors operating at 100 Gbits/s are still not widely available, so that alternative approaches to achieving a 100 Gbits/s transmission using commercially available components are currently of great interest. Such an approach based on OFDM was recently proposed by our research team [11] and will be described here for the completeness of the presentation.

Due to the fact that all state-of-the-art fiber-optic communication systems essentially use the intensity modulation/direct detection (IM/DD), we consider the LDPC-coded optical OFDM communications with DD only. The coherent optical OFDM systems [7] require the use of an additional local laser, which increases the receiver complexity. At the same time, those systems are sensitive to the laser phase noise because the OFDM symbol rate becomes comparable to the distributed feedback (DFB) laser linewidth (see [12] for more details).

The paper is organized as follows. The concept of LDPC-coded OFDM transmission is introduced in Section 2. In Section 3 we describe a class of LDPC codes suitable for OFDM. In Section 4 we discuss the use of LDPC-coded OFDM in fiber-optics communications.

## 2. LDPC-Coded OFDM Transmission

The transmitter and receiver configurations and format of the transmitted OFDM symbol are shown in Figs. 1(a)–1(c), respectively. On the transmitter side the information-bearing streams at 10 Gbits/s are encoded using identical LDPC codes. The outputs of these LDPC encoders are further demultiplexed and parsed into groups of $B$ bits corresponding to one OFDM frame. The $B$ bits in each OFDM frame are subdivided into $K$ subchannels with the $i$th subcarrier carrying $b_i$ bits, $B=\Sigma b_i$.

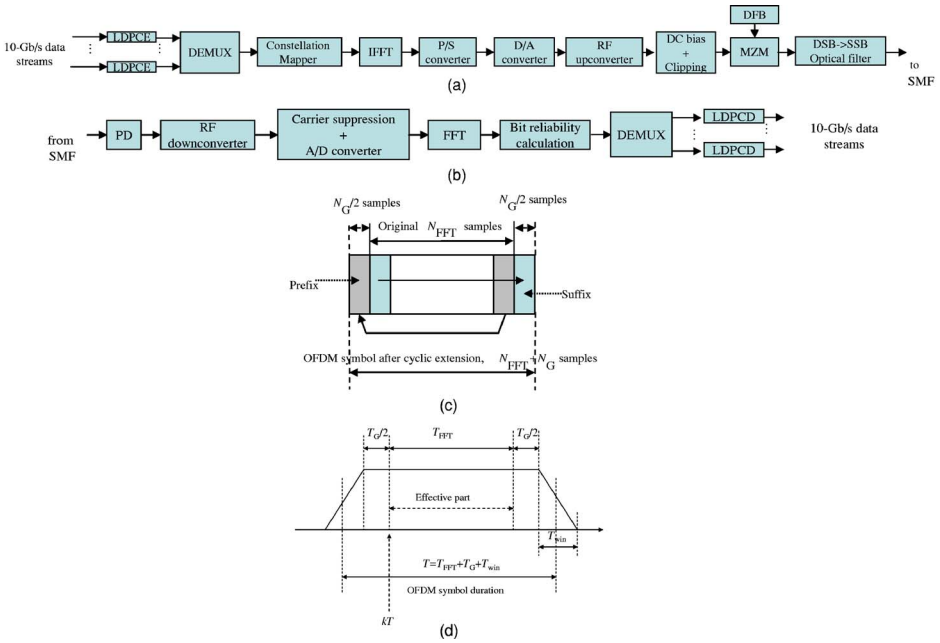


Fig. 1. (a) Transmitter configuration, (b) receiver configuration, (c) OFDM symbol after cyclic extension, and (d) OFDM symbol after windowing. LDPCE-LDPC, encoder; LDPCD-LDPC, decoder; S/P, serial-to-parallel converter; MZM, Mach–Zehnder modulator; SMF, single-mode optical fiber; PD, photodetector; DSB, double sideband; SSB, single sideband.

The $b_i$ bits from the $i$th subchannel are mapped into a complex-valued signal from a $2^{b_i}$-point signal constellation such as quadrature amplitude modulation (QAM), which is the example constellation considered in this paper. For example, $b_i=2$ for quaternary phase shift keying (QPSK) and $b_i=4$ for 16 QAM. The complex-valued signal points from subchannels are considered to be the values of the discrete Fourier transform (DFT) of a multicarrier OFDM signal. By selecting the number of subchannels $K$, sufficiently large, the OFDM symbol interval can be made significantly larger than the dispersed pulse width of an equivalent single-carrier system. This spreading of the symbol interval results in ISI reduction. The OFDM symbol, shown in Fig. 1(c), is generated as follows: $N_{\mathrm{QAM}}(=K)$ input QAM symbols are zero padded to obtain $N_{\mathrm{FFT}}$ input samples for inverse fast Fourier transform (IFFT), $N_G$ nonzero samples are inserted (as explained below) to create the guard interval, and the OFDM symbol is multiplied by the window function. The OFDM symbol windowing is illustrated in Fig. 1(d). The purpose of cyclic extension is to preserve the orthogonality among subcarriers even when the neighboring OFDM symbols partially overlap due to dispersion, and the role of windowing is to reduce the out-of-band spectrum. For efficient chromatic dispersion compensation, the length of the cyclically extended guard interval should be smaller than the total chromatic dispersion spread.

The cyclic extension, illustrated in Fig. 1(c), is accomplished by repeating the last $N_G/2$ samples of the effective OFDM symbol part ($N_{\mathrm{FFT}}$ samples) as a prefix and repeating the first $N_G/2$ samples as a suffix. After digital-to-analog (D/A) conversion and RF upconversion, the RF signal can be mapped to the optical domain using one of two possible options: (i) the OFDM signal can directly modulate a distributed feedback (DFB) laser, or (ii) the OFDM signal can be used as the RF input of a Mach–Zehnder modulator (MZM). A "DC bias component" is added to the OFDM signal in order to enable recovery of the QAM symbols incoherently. In what follows, three different OFDM schemes are introduced. The first scheme is based on direct modulation, and will be referred to as the "biased-OFDM" (B-OFDM) scheme. Because bipolar signals cannot be transmitted over an IM/DD link, it is assumed that the bias component is sufficiently large so that, when added to the OFDM signal, the resulting sum is nonnegative. The main disadvantage of the B-OFDM scheme is its poor power efficiency. To improve the OFDM power efficiency, two alternative schemes can be used. The first scheme, which we will refer to as the "clipped-OFDM" (C-OFDM) scheme, is based on single-sideband (SSB) transmission and clipping of the OFDM signal after bias addition. The bias is varied in order to find the optimum one for fixed optical launched power. It was found that the optimum bias is one in which ~50% of the total electrical signal energy before clipping is allocated for transmission of a carrier. The second power-efficient scheme, which we shall refer to as the "unclipped-OFDM" (U-OFDM) scheme, is based on SSB transmission using an $LiNbO_3$ MZM. To avoid distortion due to clipping at the transmitter, the information is mapped into the optical domain by modulating the electrical field of the optical carrier (instead of intensity modulation employed in the B-OFDM and C-OFDM schemes). In this way both positive and negative portions of the electrical OFDM signal are transmitted to the photodetector. Distortion introduced by the photodetector, caused by squaring, is successfully eliminated by proper filtering, and the recovered signal does not exhibit significant distortion. It is important to note, however, that the U-OFDM scheme is slightly less power efficient than that of the C-OFDM scheme. The SSB modulation can be achieved either by appropriate optical filtering of the double-sideband signal at MZM output [see Fig. 1(a)] or by using the Hilbert transformation of the in-phase component of the OFDM RF signal. The first version requires the use of only the in-phase component of the RF OFDM signal, providing that zero padding is done in the middle of the OFDM symbol rather than at the edges.

The transmitted OFDM signal can be written as

$$s(t) = s_{\mathrm{OFDM}}(t) + b, \tag{1}$$

where

$$s_{\mathrm{OFDM}}(t) = \mathrm{Re}\left\{ \sum_{k=-\infty}^{\infty} w(t-kT) \sum_{i=-N_{\mathrm{FFT}}/2}^{N_{\mathrm{FFT}}/2-1} X_{i,k} e^{j2\pi(i/T_{\mathrm{FFT}})\cdot(t-kT)} e^{j2\pi f_{\mathrm{RF}} t} \right\},$$

is defined for

$$kT - T_G/2 - T_{\text{win}} \le t \le kT + T_{\text{FFT}} + T_G/2 + T_{\text{win}}.$$

In the above expression $X_{i,k}$ denotes the $i$th subcarrier of the $k$th OFDM signal, $w(t)$ is the window function, and $f_{\text{RF}}$ is the RF carrier frequency. The duration of the OFDM symbol is denoted by $T$, while $T_{\text{FFT}}$ is the fast Fourier transform (FFT) sequence duration, $T_G$ is the guard interval duration (the duration of cyclic extension), and $T_{\text{win}}$ denotes the windowing interval duration; $b$ denotes the DC bias component, which is introduced to enable the OFDM demodulation using the direct detection.

High-speed optical receivers commonly employ the transimpedance design, which is a good compromise between noise and bandwidth. A preamplified positive intrinsic negative (PIN) photodiode, or an avalanche photodiode, is typically used as an optical detector. The PIN photodiode output current can be written as

$$\begin{aligned} i(t) &= \mathsf{R}|(s_{\text{OFDM}}(t) + b) * h(t)|^2 \\ &= \mathsf{R}[|s_{\text{OFDM}}(t) * h(t)|^2 + |b * h(t)|^2 + 2R_e\{(s_{\text{OFDM}}(t) * h(t))(b * h(t))\}], \end{aligned} \tag{2}$$

where $s_{\text{OFDM}}(t)$ denotes the transmitted OFDM signal in the RF domain, upon D/A conversion and RF upconversion, already introduced by Eq. (1); $b$ is the DC bias component, and $\mathsf{R}$ denotes the photodiode responsivity. The impulse response of the optical channel is represented by $h(t)$. We modeled this channel by solving the nonlinear Schrödinger equation numerically using the split-step Fourier method as described in [21]. The signal after RF downconversion and appropriate filtering can be written as

$$r(t) = [i(t)k_{\text{RF}} \cos(\omega_{\text{RF}}t)] * h_e(\tau) + n(t), \tag{3}$$

where $h_e(t)$ is the impulse response of the low-pass filter (having the transfer function $H_e(j\omega)$), $n(t)$ is electronic noise in the receiver, and $k_{\text{RF}}$ denotes the RF downconversion coefficient. Finally, after the analog-to-dialog (A/D) conversion and cyclic extension removal, the signal is demodulated by using the FFT algorithm. The soft outputs of the FFT demodulator are used to estimate the bit reliabilities that are fed to identical LDPC iterative decoders implemented based on the sum–product algorithm [22,23].

For the sake of illustration, let us consider the signal waveforms and power-spectral densities (PSDs) at various points in the OFDM system given in Fig. 1. These examples were generated using SSB transmission in a back-to-back configuration. The bandwidth of the OFDM signal is set to $B$ GHz, and the RF carrier to $0.75B$. With $B$ we denoted the aggregate data rate. The number of OFDM subchannels is set to 64, the OFDM sequence is zero padded, and the FFT is calculated using 128 points. The guard interval is obtained by a cyclic extension of $2 \times 16$ samples. The average transmitted launched power is set to 0 dBm. The OFDM transmitter parameters are carefully chosen such that the RF driver amplifier and MZM operate in linear regime [see Figs. 2(a)–2(c)]. The PSDs of the MZM output signal and the photodetector output sig-

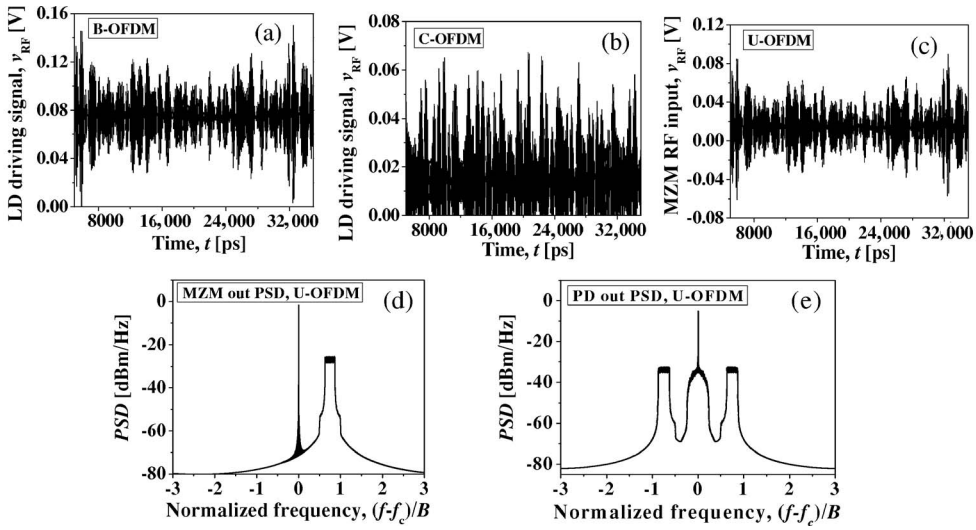


Fig. 2. Waveforms and PSDs of SSB QPSK-OFDM signal at different points during transmission for the electrical signal-to-noise ratio (SNR) (per bit) of 6 dB. ($f_c$, the optical carrier frequency; LD, the laser diode.)

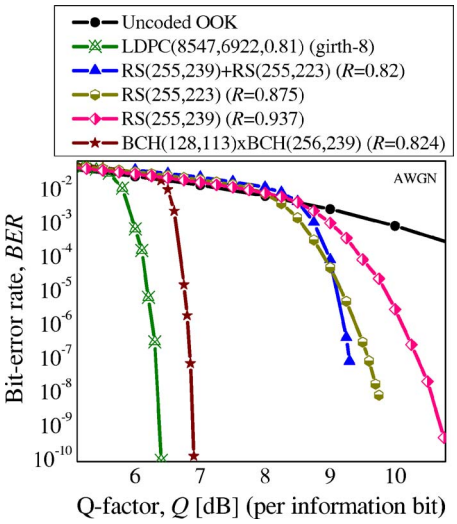


Fig. 3. BIBD LDPC codes against RS, concatenated RS, and turboproduct codes.

nal are shown in Figs. 2(d) and 2(e), respectively. The OFDM term after beating in the PD, the low-pass term, and the squared OFDM term can easily be identified.

## 3. Girth-8 BIBD LDPC Codes

Now we turn our attention to the selection of LDPC codes [22–25]. The codes employed in this paper are based on combinatorial objects known as balanced-incomplete block designs (BIBDs) [26]. A balanced-incomplete balanced design, denoted as BIBD $(v,k,\{0,1,\ldots,\lambda\})$ is a collection of subsets (blocks) of a $v$-set $V$ with a size of each block $k \leq v$, so that each pair of elements occurs in at most $\lambda$ of the blocks. It should be noticed that we have relaxed the constraint in the definition of BIBD from [26] by replacing the word exact with at most. The purpose of this relaxation is to increase the number of possible BIBDs that result in LDPC codes of high code rates. To increase the girth to 8, certain blocks from a BIBD are to be removed. To design the girth-8 LDPC codes we employed the algorithm we introduced in [25].

In Fig. 3 the bit error rate (BER) performance of girth-8 BIBD LDPC code (for 30 iterations in the sum–product decoding algorithm) is compared against Reed–Solomon (RS), concatenated RS, and turboproduct codes. $R=0.81$ LDPC code outperforms $R=0.824$ turboproduct code by more than 0.5 dB at BER of $10^{-8}$ and outperforms the concatenated RS code ($R=0.82$) by ~3 dB.

## 4. LDPC-Coded OFDM Fiber-Optics Communications

The main reasons for suitability of the OFDM for long-haul transmission are [6]: (i) improvement of spectral efficiency, (ii) simplification of the chromatic dispersion compensation engineering, and (iii) PMD compensation [12]. We have shown in [5] that U-OFDM provides the best power efficiency-BER performance compromise and, as such, is adopted here. The BER performance of this scheme (with aggregate data rate 40 Gbits/s) against the conventional LDPC-coded RZ-OOK scheme (operating at 40 Gbits/s) is given in Fig. 4 for the linear channel model. The LDPC-coded QPSK U-OFDM provides more than 2 dB coding gain improvement over the LDPC coded RZ-OOK at BER of $10^{-8}$. We have shown in [6] that LDPC-coded OFDM provides much higher spectral efficiency than LDPC-coded RZ-OOK.

Another possible application in fiber-optics communications is 100 Gbits/s Ethernet [11]. For example, for QPSK OFDM transmission two 1 Gbits/s streams create a QPSK signal constellation point; with 50 subcarriers carrying 2 Gbits/s traffic, the aggregate rate of 100 Gbits/s can be achieved.

The BER curves for the uncoded 100 Gbits/s OFDM SSB transmission using QPSK are shown in Fig. 5 for the dispersion map described in Fig. 6 and fiber parameters given in Table 1. The dispersion map is composed of $N$ spans of length $L=120$ km, consisting of $2L/3$ km of the $D_+$ fiber followed by $L/3$ km of the $D_-$ fiber,

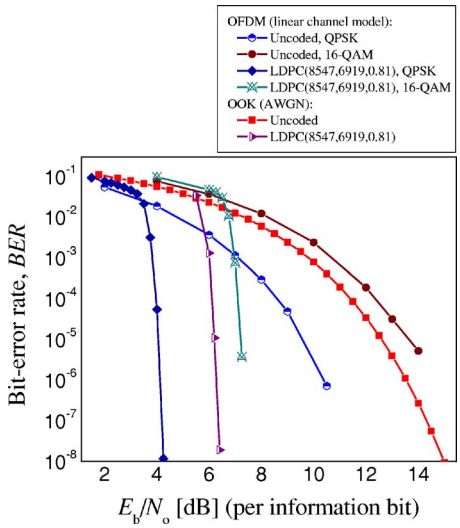


Fig. 4. BER performance of OFDM against OOK for a linear channel model.

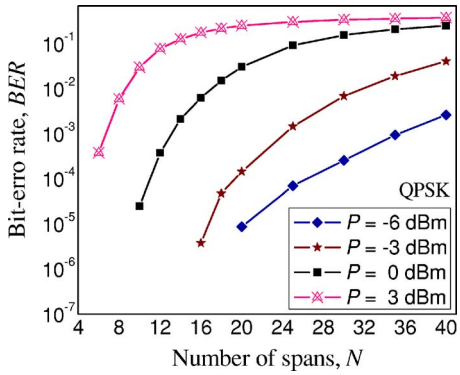


Fig. 5. Uncoded BER versus number of spans for SSB QPSK OFDM transmission for the dispersion map in Fig. 6.

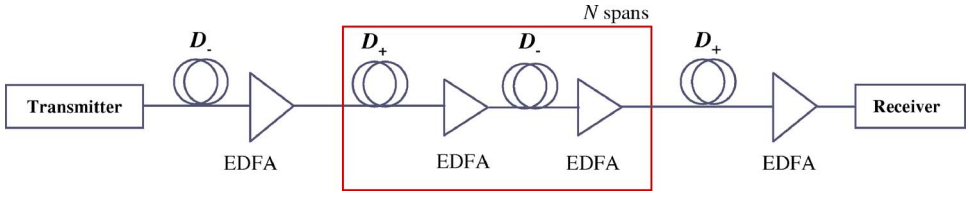


Fig. 6. Dispersion map under study.

**Table 1. Fiber Parameters**

| | $D_+$ Fiber | $D_-$ Fiber |
|---|---|---|
| Dispersion [ps/(nm km)] | 20 | −40 |
| Dispersion slope [ps/(nm$^2$ km)] | 0.06 | −0.12 |
| Effective cross-sectional area [$\mu$m$^2$] | 110 | 50 |
| Nonlinear refractive index [m$^2$/W] | $2.6\times10^{-20}$ | $2.6\times10^{-20}$ |
| Attenuation coefficient [dB/km] | 0.19 | 0.25 |

with precompensation of −1600 ps/nm and corresponding postcompensation. The propagation of a signal through the transmission media is modeled by a nonlinear Schrödinger equation (NLSE) [21],

$$\frac{\partial A}{\partial z} = -\frac{\alpha}{2}A - \frac{i}{2}\beta_2\frac{\partial^2 A}{\partial T^2} + \frac{\beta_3}{6}\frac{\partial^3 A}{\partial T^3} + i\gamma\left(|A|^2 - T_R\frac{\partial |A|^2}{\partial T}\right)A, \tag{4}$$

where $z$ is the propagation distance along the fiber, relative time, $T=t-z/v_g$, gives a frame of reference moving at the group velocity $v_g$, $A(z,T)$ is the complex field amplitude of the pulse, $\alpha$ is the attenuation coefficient of the fiber, $\beta_2$ is the group velocity dispersion (GVD) coefficient, $\beta_3$ is the second-order GVD, and $\gamma$ is the nonlinearity coefficient giving rise to Kerr effect nonlinearities. Such nonlinearities include self-phase modulation (SPM), IWFM, IXPM, cross-phase modulation (XPM), and FWM. $T_R$ denotes the Raman coefficient describing the stimulated Raman scattering (SRS). The NLSE was solved using the split-step Fourier method [21].

From Fig. 5 it is evident that 100 Gbits/s transmission over 3840 km is possible using OFDM and LDPC codes with threshold BER of $10^{-2}$ (for launched power of −3 dBm). For more details an interested reader is referred to our recent paper [11].

In the presence of PMD, the PIN photodiode output current can be written as follows:

$$i(t) = \mathrm{R}\{|\sqrt{k}(s_{\mathrm{OFDM}}(t)+b) * h_V(t)|^2 + |\sqrt{1-k}(s_{\mathrm{OFDM}}(t)+b) * h_H(t)|^2\}, \tag{5}$$

where $k$ denotes the power-splitting ratio between two principal states of polarizations (PSPs). For the first order PMD, the optical channel responses $h_H(t)$ and $h_V(t)$ of horizontal and vertical PSPs are given as [12] $h_H(t)=\delta(t+\Delta\tau/2)$ and $h_V(t)=\delta(t-\Delta\tau/2)$, respectively, where $\Delta\tau$ is the DGD of two PSPs. From [12] it follows that in the presence of the first order PMD, the photodiode output signal, after appropriate filtering to remove the squared and DC terms, is proportional to

$$i(t) \sim 2\mathrm{R}b[ks_{\mathrm{OFDM}}(t-\Delta\tau/2) + (1-k)s_{\mathrm{OFDM}}(t+\Delta\tau/2)]. \tag{6}$$

Equation (6) reminds to a two-ray multipath wireless model [1], and therefore, the channel estimation techniques similar to those employed in wireless communications are straightforwardly applicable here. It can be shown that the received QAM symbol of $i$th subcarrier of the $k$th OFDM symbol is related to the transmitted QAM symbol $X_{i,k}$ by

$$Y_{i,k} = h_i e^{j\theta_k} X_{i,k} + n_{i,k}, \tag{7}$$

where $h_i$ is the channel distortion introduced by PMD (and chromatic dispersion) and $\theta_i$ is the phase shift of the $i$th subcarrier due to chromatic dispersion and SPM. Notice that in the absence of chromatic dispersion and SPM, $\theta_i$ is actually equal to zero. Therefore, to determine the PMD distortion coefficients $h_i$ it is not necessary to transmit the pilot tones. It is enough to pretransmit just the short training OFDM sequence. In a decision-directed mode the transmitted QAM symbols are estimated by

$$\hat{X}_{i,k} = (h_i^*/|h_i|^2)e^{-j\theta_k}Y_{i,k}. \tag{8}$$

The signal constellation diagrams, after the demapper from Fig. 1, and before and after applying the channel estimation are shown in Figs. 7(a) and 7(b). They correspond to the worst-case scenario ($k=1/2$) and 10 Gbits/s aggregate data rate. Therefore, the channel estimation based OFMD is able to compensate for DGD of 1600 ps. Notice that for the thermal noise dominated scenario the estimated coefficients in Eq. (8) are expected to be more accurate than that for the amplified spontaneous emission (ASE) noise dominated scenario.

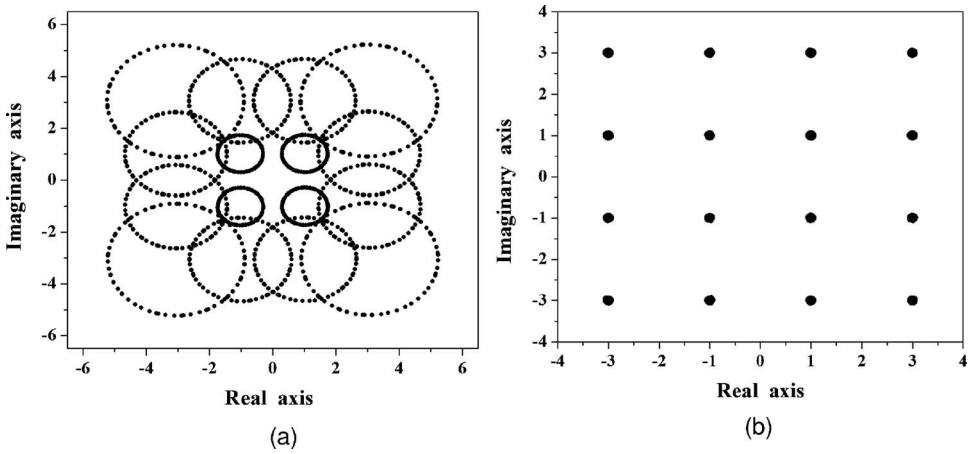


Fig. 7. (a) Signal constellation diagram before PMD compensation for DGD of 1600 ps, and (b) signal constellation diagram after PMD compensation (other effects except PMD have been ignored).

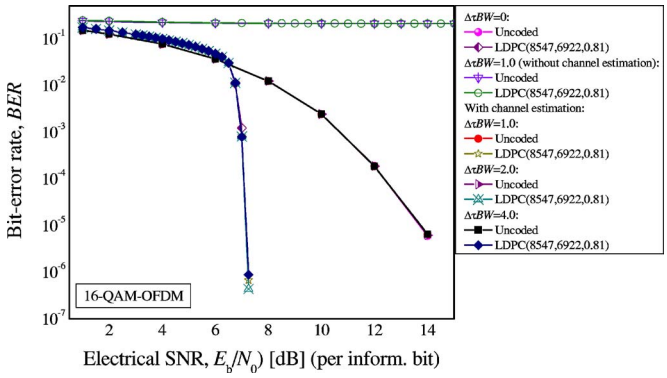


Fig. 8. BER performance of LDPC(8547,6922)-coded 16-QAM-OFDM for different DGD values, and thermal noise dominated scenario. The power-splitting ratio between two PSPs was set to $k=1/2$.

The results of PMD simulations for U-OFDM and thermal noise dominated scenario are shown in Fig. 8 for different DGDs, and the worst-case scenario ($k=1/2$). The OFDM signal bandwidth is set to BW$=0.25B$ ($B$ is the aggregate bit rate set to 10 Gbits/s), the number of subchannels is set to $N_{\mathrm{QAM}}=64$, FFT/IFFT is calculated in $N_{\mathrm{FFT}}=128$ points, RF carrier frequency is set to $0.75B$, the bandwidth of optical filter for SSB transmission is set to $2B$, and the total averaged launched power is set to 0 dBm. The guard interval is obtained by cyclic extension of $N_G=2\times16$ samples. The Blackman–Harris windowing function is applied, and the OFDM symbol period is 0.06544 $\mu$s. The 16-QAM-OFDM with and without channel estimation is observed in simulations. The effect of PMD is reduced by: (i) using a sufficient number of subcarriers so that the OFDM symbol rate is significantly lower than aggregate bit rate, and (ii) using the short training sequence to estimate the PDM distortion. For DGD of 1/BW the RZ-OOK threshold receiver is not able to operate properly at all, because it enters the BER error floor. Notice that 16-QAM-OFDM without channel estimation enters the BER floor, and even advanced forward error correction (FEC) cannot help too much in reducing the BER.

The similar channel estimation technique can be used to compensate for the phase rotation due to SPM [6,11]. For example, the signal constellation diagrams before and after SPM phase correction are shown in Figs. 9(a) and 9(b) for the transmission distance of 1200 km, for the dispersion map given in Fig. 6, and aggregate data rate of 100 Gbits/s. The four pilot tones were sufficient to cancel the phase rotation due to SPM. The similar equalization scheme can be used for intermodal dispersion compensation [9] and chromatic dispersion compensation [7,8,14,15].

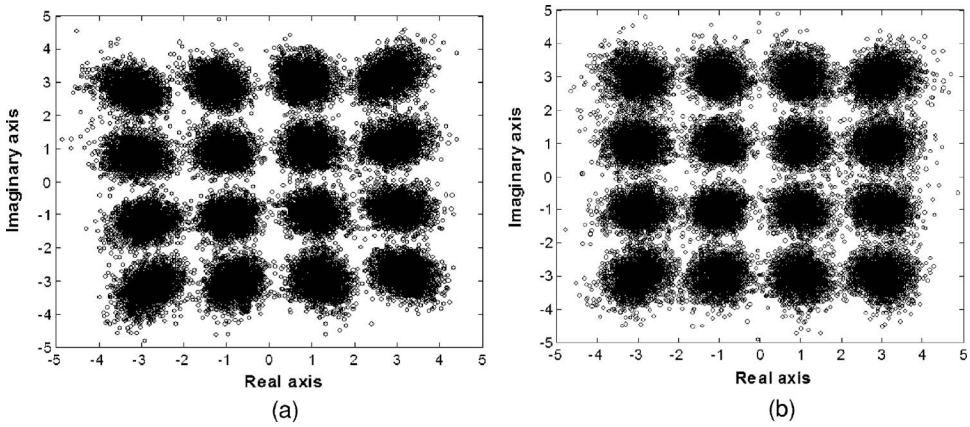


Fig. 9. Received signal constellation for 16-QAM SSB transmission after 1200 km for the dispersion map in Fig. 6, and aggregate data rate of 100 Gbits/s: (a) before SPM phase correction, and (b) after the SPM phase correction.

## 5. Summary

The LDPC-coded OFDM was considered in context of long-haul optical communication systems and 100 Gbits/s Ethernet. The OFDM is an excellent chromatic dispersion and PMD compensation candidate. Based on the pilot-aided channel estimation, it is capable of compensating DGD of even 1600 ps, for thermal noise limited channel. The similar channel estimation can be used to compensate for the common phase error due to SPM. However, the intercarrier interference (ICI) due to FWM among subcarriers cannot be eliminated by pilot-aided channel estimation, and remains as an important performance degradation factor to be addressed in the future. Some initial results in this direction have been recently presented by Lowery [27].

## Acknowledgment

This work was supported in part by the National Science Foundation (NSF) under grants IHCS-0725405 and ITR 0325979.

## References

1. R. Prasad, *OFDM for Wireless Communications Systems* (Artech House, 2004).
2. Y. Wu and B. Caron, "Digital television terrestrial broadcasting," IEEE Commun. Mag. **32**, 46–52 (1994).
3. A. Kim, Y. Hun Joo, and Y. Kim, "60 GHz wireless communication systems with radio-over fiber links for indoor wireless LANs," IEEE Trans. Consum. Electron. **50**, 517–520 (2004).
4. I. B. Djordjevic, B. Vasic, and M. A. Neifeld, "LDPC coded orthogonal frequency division multiplexing over the atmospheric turbulence channel," in *Conference on Lasers and Electro-Optics/Quantum Electronics and Laser Science Conference and Photonic Applications Systems Technologies*, Technical Digest (CD) (Optical Society of America, 2006), paper CMDD5.
5. I. B. Djordjevic, B. Vasic, and M. A. Neifeld, "LDPC coded OFDM over the atmospheric turbulence channel," Opt. Express **15**, 6332–6346 (2007).
6. I. B. Djordjevic and B. Vasic, "Orthogonal frequency-division multiplexing for high-speed optical transmission," Opt. Express **14**, 3767–3775 (2006).
7. W. Shieh and C. Athaudage, "Coherent optical frequency division multiplexing," Electron. Lett. **42**, 587–589 (2006).
8. A. J. Lowery, L. Du, and J. Armstrong, "Orthogonal frequency division multiplexing for adaptive dispersion compensation in long haul WDM systems," *Optical Fiber Communication Conference and Exposition and The National Fiber Optic Engineers Conference*, Technical Digest (CD) (Optical Society of America, 2006), paper PDP39.
9. A. J. Lowery and J. Armstrong, "10 Gb/s multimode fiber link using power-efficient orthogonal-frequency-division multiplexing," Opt. Express **13**, 10003–10009 (2005).
10. I. B. Djordjevic, "LDPC-coded OFDM transmission over graded-index plastic optical fiber links," IEEE Photon. Technol. Lett. **19**, 871–873 (2007).
11. I. B. Djordjevic and B. Vasic, "100 Gb/s transmission using orthogonal frequency-division multiplexing," IEEE Photon. Technol. Lett. **18**, 1576–1578 (2006).
12. I. B. Djordjevic, "PMD compensation in fiber-optic communication systems with direct detection using LDPC-coded OFDM," Opt. Express **15**, 3692–3701 (2007).
13. W. Shieh, "PMD-supported coherent optical OFDM systems," IEEE Photon. Technol. Lett. **19**, 134–136 (2006).

14. S. L. Jansen, I. Morita, N. Takeda, and H. Tanaka, "20-Gb/s OFDM transmission over 4,160-km SSMF enabled by RF-pilot tone phase compensation," in *National Fiber Optic Engineers Conference*, OSA Technical Digest Series (CD) (Optical Society of America, 2007), paper PDP15.
15. B. J. Schmidt, A. J. Lawery, and J. Amstrong, "Experimental demonstrations of 20 Gbit/s direct-detection optical OFDM and 12 Gbit/s with a colorless transmitter," *Optical Fiber, Communication Conference and Exposition and The National Fiber Optic Engineers Conference*, OSA Technical Digest Series (CD) (Optical Society of America, 2007), paper PDP18.
16. I. B. Djordjevic, H. G. Batshon, M. Cvijetic, L. Xu, and T. Wang, "PMD compensation by LDPC-coded turbo equalization," IEEE Photon. Technol. Lett. **19**, 1163–1165 (2007).
17. I. B. Djordjevic and B. Vasic, "Constrained coding techniques for the suppression of intrachannel nonlinear effects in high-speed optical transmission," J. Lightwave Technol. **24**, 411–419 (2006).
18. A. Zapata, M. Düser, J. Spencer, P. Bayvel, I. de Miguel, D. Breuer, N. Hanik, and A. Gladisch, "Next-generation 100-gigabit metro Ethernet (100 GbME) using multiwavelength optical rings," J. Lightwave Technol. **22**, 2420–2434 (2004).
19. M. Duelk, "Next generation 100 G Ethernet," in *31st European Conference on Optical Communication* (IEE, 2005), paper Tu3.1.2, pp. 25–29.
20. G. Raybon, P. J. Winzer, and C. R. Doerr, "10 × 107-Gb/s electronically multiplexed and optically equalized NRZ transmission over 400 km," in *Optical Fiber Communication Conference and Exposition and The National Fiber Optic Engineers Conference*, Technical Digest (CD) (Optical Society of America, 2006), paper PDP32.
21. G. P. Agrawal, *Nonlinear Fiber Optics* (Academic, 2001).
22. C.-C. Lin, K.-L. Lin, H.-Ch. Chang, and C.-Y. Lee, "A 3.33 Gb/s (1200,720) low-density parity check code decoder," in *Proceedings of the 31st European Solid-State Circuits Conference 2005* (IEEE, 2005), pp. 211–214.
23. I. B. Djordjevic, S. Sankaranarayanan, S. K. Chilappagari, and B. Vasic, "Low-density parity-check codes for 40 Gb/s optical transmission systems," IEEE J. Sel. Top. Quantum Electron. **12**, 555–562 (2006).
24. I. B. Djordjevic and B. Vasic, "MacNeish–Mann theorem based iteratively decodable codes for optical communication systems," IEEE Commun. Lett. **8**, 538–540 (2004).
25. B. Vasic, I. B. Djordjevic, and R. Kostuk, "Low-density parity check codes and iterative decoding for long haul optical communication systems," J. Lightwave Technol. **21**, 438–446 (2003).
26. I. Anderson, *Combinatorial Designs and Tournaments* (Oxford U. Press, 1997).
27. A. Lowery, "Nonlinearity and its compensation in optical OFDM systems," presented at *33rd European Conference on Optical Communication, Workshop 5, Berlin, Germany, 16–20 Sept. 2007* (Electronic signal processing for transmission impairment mitigation: future challenges).